Time delays in heavy-ion-induced fission of medium-Z nuclei, measured by crystal blocking

J. U. Andersen and J. Chevallier

Department of Physics, University of Aarhus, DK-8000 Aarhus C, Denmark

J. S. Forster

Département de Physique, Université de Montréal, Québec H3C 3J7, Canada

S. A. Karamian

FLNR, Joint Institute for Nuclear Research, 141980 Dubna, Russian Federation

C. R. Vane, J. R. Beene, C. J. Gross, H. F. Krause, J. F. Liang, and D. Shapira

Oak Ridge National Laboratory, Oak Ridge, Tennessee 37831, USA

A. Uguzzoni

Department of Physics, University of Bologna and I.N.F.N., 40126 Bologna, Italy

Time delays in fission induced by bombardment of Mo with 170- and 180-MeV ^{32}S, 225- and 240-MeV ^{48}Ti, and 300-MeV ^{58}Ni have been measured by observation of crystal blocking of fission fragments. In contrast to earlier measurements with a W target, the results are consistent with fission of a compound nucleus in competition with mainly neutron emission. Most of the fissions happen on a time scale much shorter than attoseconds but there is a significant component of fission with much longer lifetimes. The measurements are reproduced with a standard statistical model, including a Kramers correction to fission widths from the viscosity of hot nuclear matter. These new results support the interpretation of our earlier measurements with a W target, which indicate that there is a transition in heavy-ion-induced fission at large atomic number and mass, from multichance fission in the standard Bohr-Wheeler picture to fission without formation of a compound nucleus. The process is slowed down by nuclear viscosity, with measured delays of order attoseconds.

I. INTRODUCTION

This paper describes the continuation of a series of experiments [1–3] on lifetimes of heavy-ion-induced fission using the crystal-blocking technique [4]. For fission of high-Z nuclei ($Z = 90$–106), we found the surprising result that the fission decay is characterized by a single lifetime of order 1 attosecond (as). This is in contrast to previous results for light-ion-induced fission [5–11] which were consistent with a description by multichance fission of a compound nucleus [12] with a broad distribution of lifetimes. The new results were interpreted as fission dominated by viscosity [13], "fission by diffusion," which is closely related to the description of formation of a compound nucleus in heavy-ion reactions as "fusion by diffusion" [14]. This interpretation is a radical departure from the standard Bohr-Wheeler description with competition between fission and neutron emission in a compound nucleus in statistical equilibrium.

In our previous experiments a thin W ($Z = 74$) crystal grown epitaxially on a Mo/MgO backing was used as target, and this was replaced by a Mo/MgO target with $Z = 42$ and a broad distribution of isotopes, from $A = 92$ to 100 with average $A = 96$. As before, ion beams of ^{32}S, ^{48}Ti, and ^{58}Ni bombarded the target, leading to merged nuclei with atomic numbers $Z = 58$, 64, and 70. The physics of the fission process in the present experiment differs markedly from that of the high-Z nuclei studied in Refs. [1–3]. The basic description

developed in the 1970s is based on the rotating-liquid-drop model (RLDM) [15]. The fission barrier is very high at zero angular momentum, I, but decreases strongly with increasing I values. For I that is not too high, the barrier configuration is quite extended and, in contrast to the high-Z nuclei studied in the earlier experiments, the deformation at the barrier is larger than for the initial configuration of two touching nuclei. This favors formation of a compound nucleus before fission [14]. For small I values the fused nucleus survives more or less intact and becomes an evaporation residue (ER), while the nucleus fissions with high probability at high I values [16]. In a number of studies of cross sections for fission and for ER formation it was found that agreement with statistical modeling requires a reduction of the RLDM fission barrier by 30%–45% [17–19], and this was interpreted as an effect of the finite range of nuclear forces [20,21].

A crucial question for the delay of the fission process is the role of nuclear viscosity, characterized often by a combined friction, inertia, and stiffness parameter η [22]. The classical Kramers correction to the fission width [23], a reduction factor ($\sqrt{1 + \eta^2} - \eta$), can be important for the competition between neutron emission and fission and, hence, for the relative amount of late-chance fission with long lifetimes. With increasing η the relative contribution of late-chance fission is enhanced. Also, the reduction of the fission width reduces the total width and, hence, increases the lifetime for given angular momentum and excitation energy. However, our

earlier experiments indicated an even more important role of the viscosity for heavy-ion-induced fission of high-Z nuclei, giving an observable delay of order attoseconds for all fission events, and this could conceivably also be the case for the medium-Z nuclei.

As it turns out, our data taken with the Mo target do not show such a delay, setting an upper limit of a few times 10^{-19} s for the lifetime of early-chance fission. However, we do observe a significant component (10%–20% for S and Ti bombardment) of fission with lifetimes longer than 1 as. This is consistent with the Bohr-Wheeler picture of multichance fission for these reactions. We have made statistical calculations similar to those described in Ref. [1] and find that a viscosity parameter $\eta \sim 1$–3 is needed to reproduce the measurements. For Ni bombardment we do not observe any long-lifetime component, and this is consistent with the calculations which indicate that this component should be small. The observation of blocking dips without narrowing from lifetime effects, with the same technique and apparatus as in Ref. [3], underpins the interpretation there of the narrower blocking dips observed for bombardment of a W target.

FIG. 1. Experimental setup.

II. EXPERIMENTAL DETAILS

The measurements were carried out at the Holifield Radioactive Ion Beam Facility (HRIBF) with stable beams from the 25-MV tandem accelerator. Data were collected for beams of ^{32}S ions at 45, 150, 170, and 180 MeV, ^{48}Ti ions at 225 and 240 MeV, and ^{58}Ni ions at 100, 285, and 300 MeV incident on a thin epitaxial Mo/MgO crystal. In addition, we made short runs on a thin W crystal on Mo/MgO with 400- and 450-MeV ^{74}Ge beams.

Elastically scattered ions and fission fragments were detected in a large-solid-angle ionization detector [24] with an entrance aperture of 8 cm × 8 cm at 51.5 cm from the target. To ensure that particles entering the detector did not strike the electrodes or the sides of the detector an aperture of 3.8 cm × 3.8 cm was placed 33.7 cm from the target, resulting in a solid angle of 12.7 msr and an acceptance angle of $\pm 3.2°$ in x and in y about the center of the aperture. A schematic layout of the experimental setup is shown in Fig. 1. The anode of the detector is split into two electrodes. The first (12 cm long) gives a ΔE signal and the second (18 cm long) gives an $E_{r\,\mathrm{est}}$ signal. The total energy deposited in the counter is the sum $\Delta E + E_{\mathrm{rest}}$. The detector has the capability to determine the position (x,y) where the detected particle entered the counter. This is achieved with a cathode electrode in the shape of a backgammon. An x signal is obtained from the signals from the left (l) and right (r) sections as the ratio $(l - r)/(l + r)$. Since the signal from the cathode is dependent on the distance of the trajectory of the detected particle from the cathode (the closer to the cathode the bigger the signal) a y signal is obtained from the ratio of the cathode and anode signals, i.e., as $(l + r)/(\Delta E + E_{\mathrm{rest}})$. The x and y coordinates of the particle at the entrance are then determined from the x and y signals through a nonlinear transformation, as described below.

The split anode provides a means of particle identification from a plot of ΔE versus E_{rest}, as shown in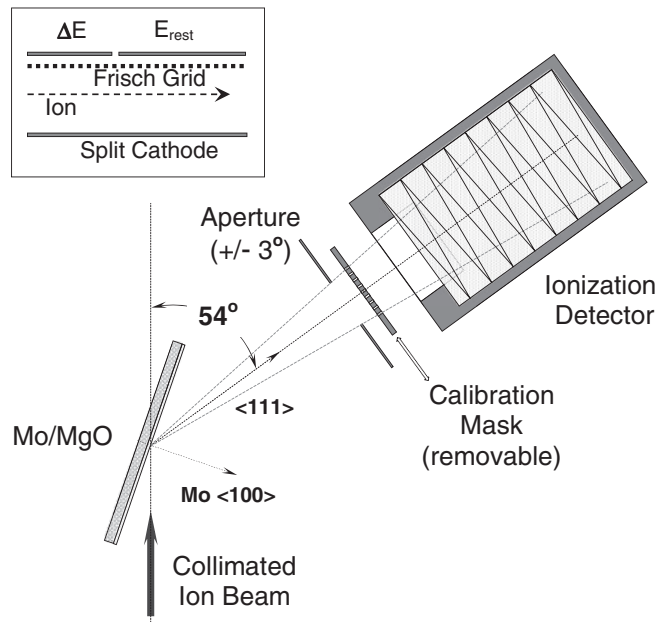 Fig. 2 for the four beams used in this work bombarding the crystal target. The isobutane gas pressure in the counter was 25 Torr for ^{32}S and ^{74}Ge beams and 15 Torr for ^{48}Ti and ^{58}Ni beams. Regions of the plots included in the blocking analysis of fission fragments are marked. The light particles appearing as nearly horizontal lines in the lower part of the plots come mainly from reactions within the thick substrate. The ions scattered elastically from Mo (or from W in the case of the ^{74}Ge beam) appear as a small circle because of the small energy loss in the thin target. Since the gas pressure is low the light reaction products such as elastically scattered ions do not at the highest energies stop in the detector, and the ΔE versus E_{rest} plots shows that these lines fold back. At the left-hand side of the plot for ^{48}Ti and ^{58}Ni beams there is a ridge of counts with a positive slope of ΔE versus E_{rest}. This arises from recoiling Mo atoms. In the plot for ^{74}Ge we see both W and Mo recoils and fission fragments from W as well as Mo. For fission in Mo the kinematics allowed only the lighter fragments to be detected, so most of the fission fragments appear below the $Z = 32$ line. The ^{74}Ge data provided a means to identify the position of this line in the ΔE versus E_{rest} spectra for the ^{48}Ti and ^{58}Ni beams, and this allowed a check of the calculations from kinematics of the mass and Z values of fission fragments.

The gains of the ΔE and E_{rest} sections were matched using the same pulse signal into the input of each preamplifier. For the 300-MeV ^{58}Ni beam (and 400-MeV ^{74}Ge), we made measurements at both 15 and 25 Torr isobutane pressure resulting in different amounts of energy of fission fragments deposited in the two regions of the detector. The fission energy spectra for the two pressures were identical, validating our gain-matching procedure.

The blocking lifetime measurements were made with a 200-nm-thick crystal of Mo grown epitaxially on an MgO substrate with a $\langle 100 \rangle$ axis normal to its surface. The crystal was oriented with a $\langle 111 \rangle$ axis (at 35° to the crystal surface)
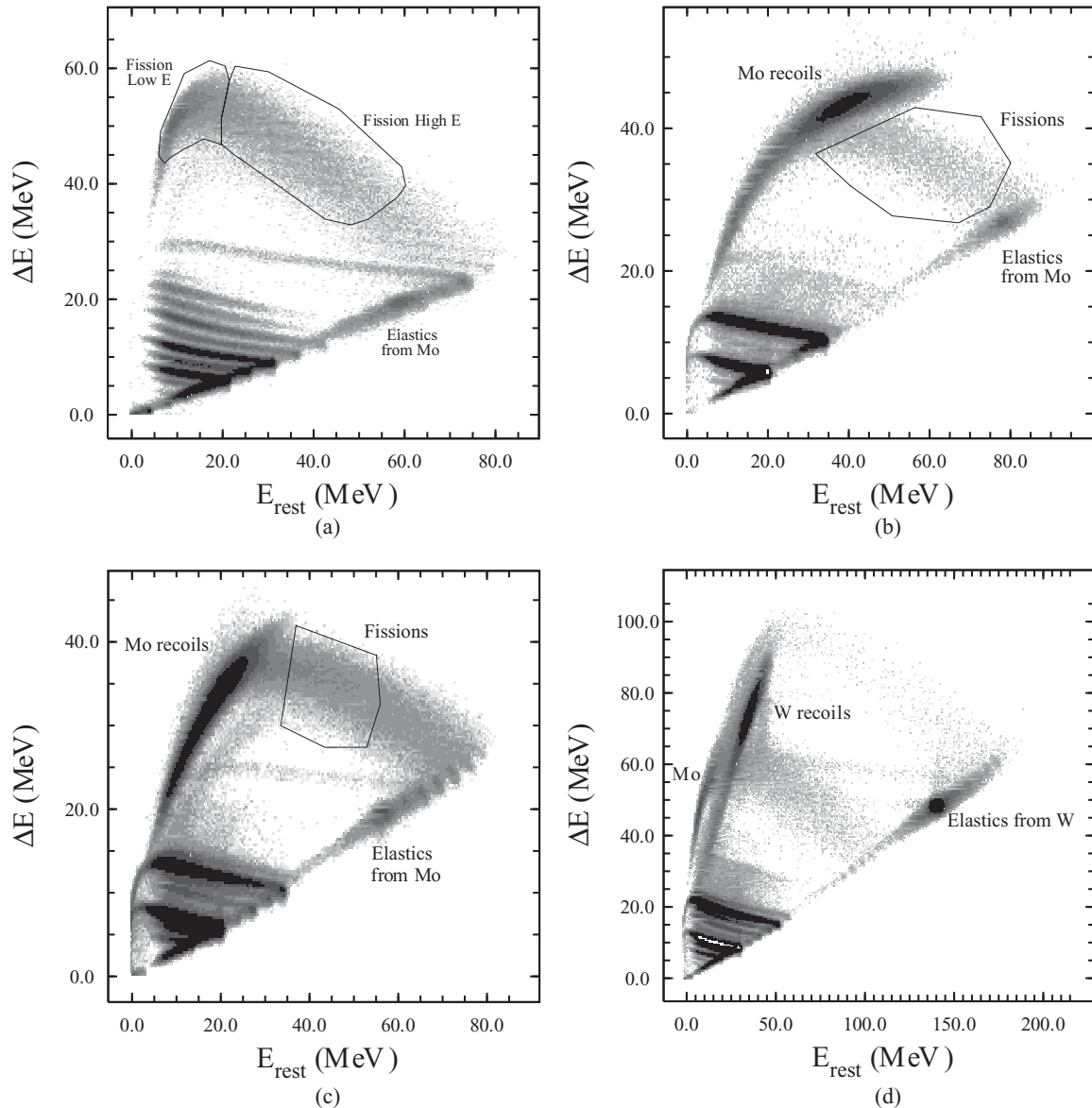
FIG. 2. 2D plots of energy losses in front and back sections of the gas counter: (a) 180-MeV ^{32}S, (b) 240-MeV ^{48}Ti, (c) 300-MeV ^{58}Ni on Mo/MgO, and (d) 450-MeV ^{74}Ge on W/Mo/MgO. The isobutane pressure in the counter was [(a) and (d)] 25 Torr and [(b) and (c)] 15 Torr. The polygons show the discrimination applied in the analysis of fission fragment blocking in the Mo epitaxial crystal.

pointing at the center of the detector. The ionization detector was positioned at 54º to the beam with the result that the beam was incident at 19º to the target surface. For the measurements with a ^{74}Ge beam the crystal consisted of 50-nm W grown on 200-nm Mo grown on MgO.

The event-by-event data consisting of ΔE, E_{rest}, l, and r were recorded on the hard disk of the data acquisition computer for later playback.

III. DATA ANALYSIS

The event-by-event data were played back with selection of events inside polygons set on the fission and elastic regions in the ΔE versus E_{rest} plot (Fig. 2). For events in the fission and elastic polygons, a 2D plot of the x and y signals was generated with the equations given above. The x and y coordinates at the entrance to the counter were obtained from a nonlinear transformation based on a set of data for elastic scattering of the beam through a mask placed in front of the detector. The mask has a square 9 × 9 array of 1.0-mm-diameter holes at 5.0 mm spacing and was placed 40.5 cm from the target. The transformation was derived from the requirement that the centroids of the "peaks" in the mask xy spectra transform into a square grid. This procedure also provides an angular calibration of the detector. Mask spectra were collected for beams of 100-MeV ^{58}Ni and 150-MeV ^{32}S.

The mask data were collected only for elastically scattered ions but were applied also for fission fragments after some

corrections. As detailed in our previous paper [3], we accounted for the fact that the y signal depends on the mass of the detected fragments, and we introduced a weak linear dependence of y on the parameter E_{rest}, ensuring that the coordinates of the center of the blocking dip were exactly the same over the whole fission region. We also corrected for the fact that the x and y signals depend on an average over the length of the counter of the x and y distances from the center line at which the particle energy is deposited as ionization [3]. For a given angle of the trajectory, the x and y signals, therefore, depend on the range of the particle. Since fission fragments have a shorter range than the elastically scattered particles used for the mask calibration, this dependence leads to a systematic underestimate of the angles for fission fragments. We, therefore, scaled the x and y signals so the limits of the aperture image for fission were equal to the limits for elastic scattering. The corrections were linear in the fraction of energy lost in the E_{rest} portion of the counter, $E_{rest}/(\Delta E + E_{rest})$, and were derived with the further condition that they should vanish for the values of ΔE and E_{rest} for elastically scattered ions. They resulted in a 5–10% "stretching" of the fission pattern in x and y about the position of the axis. A corrected xy plot for fissions from 180-MeV ^{32}S bombardment of Mo is shown in Fig. 3.

Axial blocking dips were obtained from circular averages about the blocking minimum in the xy spectra. As pointed out earlier [9], this has the advantage of improving statistical accuracy as well as eliminating, in the main, the influence of planar effects.

The lower-energy beams, 45-MeV ^{32}S and 100-MeV ^{58}Ni, stopped in the active part of the detector, giving us a means to calibrate the energy response of the detector. In addition, we have used Mo recoils from the 285- and 300-MeV ^{58}Ni beams which also stopped in the active region of the detector. A problem in the calibration is the energy loss in the target and in the 1-μm mylar foil at the entrance to the counter (up to about 6 MeV), which, for a given energy, depends on
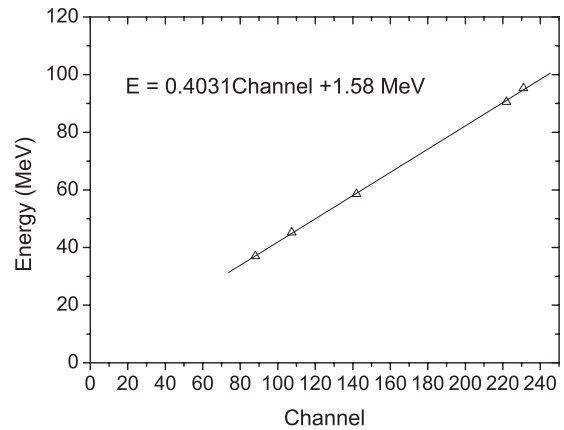
FIG. 4. Energy calibration of the counter. The points are from elastic scattering of 45-MeV ^{32}S and 100-MeV ^{58}Ni, and Mo recoils from 285 and 300 MeV ^{58}Ni.

the atomic number and mass of the particle. We have taken into account these energy losses using the SRIM stopping power tables. A linear fit to the data to determine the energy calibration is shown in Fig. 4. Since the window energy-loss corrections are nearly the same for fission fragments as for the ions used in the calibration, this curve can be used to obtain energy spectra for the fissions selected by the polygons. A comparison with calculated spectra for fission fragments is an important element of the identification of these events as fission fragments.

For the calculation of blocking dips, both the distributions in energy and in atomic number of the fragments are needed. We have calculated the relation between energy, E, and atomic number, Z, from the fission kinematics, with the assumption of a fragment charge-to-mass ratio varying linearly with mass from projectile-like to targetlike nuclei. There is a spread in Z for given mass M, as revealed by the spread in ΔE for fixed $E = E_{rest} + \Delta E$ in the 2D plots of Fig. 2, but the relative spread in E (and M) is much larger and dominates the spread in the critical angle for blocking [Eq. (4.2)]. As seen in Fig. 2(a), ions with different Z values can be identified as nearly horizontal lines just left of the elastic-scattering peak and we can easily distinguish the values from $Z = 16$ for the ^{32}S beam up to $Z = 28$. The mean Z for fission fragments calculated from kinematics is in good agreement with the value determined from this inspection of Fig. 2(a). For the ^{48}Ti and ^{58}Ni beams [Figs. 2(b) and 2(c)] the Z resolution is not as good. However, the data from the short runs with ^{74}Ge allowed us to identify the $Z = 32$ region in the ^{48}Ti and ^{58}Ni ΔE versus E_{rest} plots and compare with the average Z value for the fission fragments selected by the polygons in Figs. 2(b) and 2(c), which, according to calculations of fission kinematics, should be close to 32.
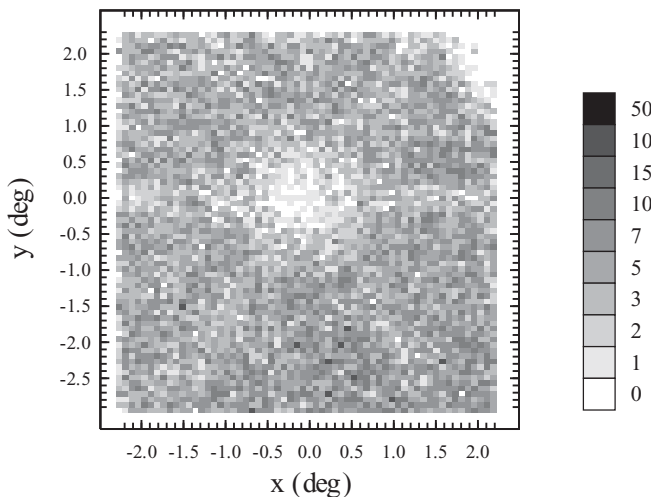
FIG. 3. Blocking pattern of fission fragments from 180-MeV ^{32}S bombarding the Mo crystal. Weak minima are visible along {110} planes intersecting at the center along a ⟨111⟩ axis, with a strong reduction in yield due to axial crystal blocking.

IV. BLOCKING DIPS FOR ELASTICS AND CALCULATIONS

A detailed description of the calculation of blocking dips was given in Ref. [3]. The main tool for the analysis has been Lindhard's continuum model [25] in which the blocking by
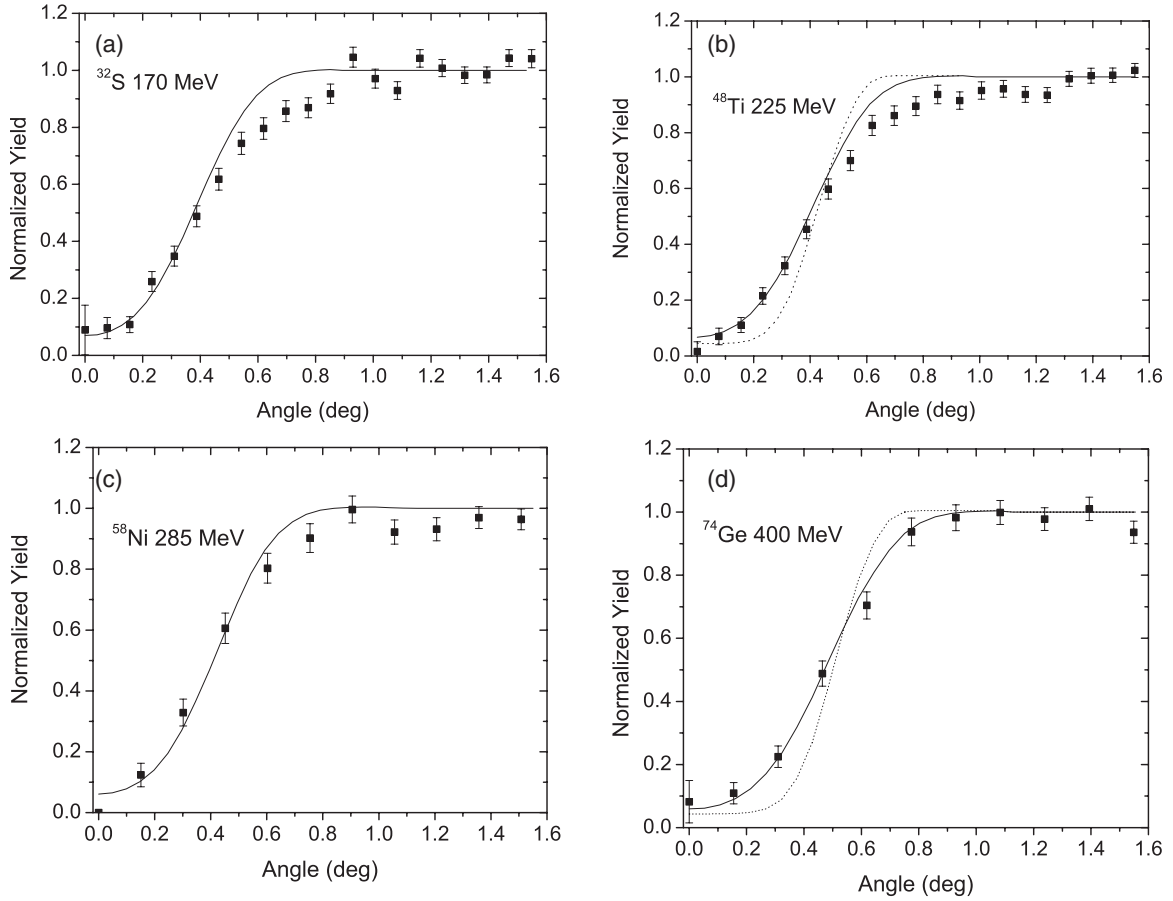
FIG. 5. Blocking dips from elastic scattering: (a) 170-MeV ^{32}S, (b) 225-MeV ^{48}Ti, (c) 285-MeV ^{58}Ni on Mo/MgO, and (d) 400-MeV ^{74}Ge on W/Mo/MgO. The full curves are from calculations based on continuum-model calculations, including corrections for beam collimation, mosaic structure, and interface strain. The dotted curves are without the correction for mosaic structure.

a string of atoms is represented by motion in an averaged, continuum axial potential. The Lindhard potential [25] has been used with a Thomas-Fermi screening radius given by

$$a_{\text{TF}} = 0.8853 a_0 (Z_1 + Z_2)^{-1/3}, \qquad (4.1)$$

where a_0 is the Bohr radius of hydrogen and Z_1 and Z_2 are the atomic numbers of the ion and the crystal atoms. The addition of Z_1 to Z_2 (for $Z_1 > Z_2/2$ only) accounts for screening of the ion-atom interaction by ion electrons [3]. The characteristic angle for the dips, approximately equal to the width at half minimum, is given by the Lindhard angle

$$\psi_1 = \left(\frac{2Z_1 Z_2 e^2}{Ed} \right)^{1/2}, \qquad (4.2)$$

where E is the ion energy and d the spacing of atoms in the strings along the crystal axis.

Measurements of blocking of elastically scattered ions are shown in Figs. 5(a)–5(d) together with the calculated dips in yield. The calculations include corrections for finite beam spot size (2 mm), for mosaic spread of microcrystals (0.3° full width at half maximum), and for strain near the crystal surfaces (4% amorphous fraction). These parameters determined from the fits to dips for elastic scattering are very close to those found earlier for the experiments with thin W crystals grown

on top of Mo/MgO [3]. For two cases calculations without the average over mosaic spread are shown (dotted curves).

The dips are reproduced except for a reduced yield just outside the dip. This is a well-known effect of multiple scattering [26,27]. Just outside the critical angle [Eq. (4.2)] the yield is strongly perturbed by planar blocking but the circular average around the axis eliminates this effect for very thin crystals. However, the higher-than-normal yield in planar shoulders is much more rapidly reduced by multiple scattering than the low yield along planes is increased, and the yield obtained from the circular average, therefore, is reduced below unity for the thicker crystals used in this experiment. In the experiment with the thinner W crystals this effect was much smaller, as seen also in the blocking dip for elastic scattering of 400-MeV ^{74}Ge on W recorded in the present experiment [Fig. 5(d)].

The square of the angular width of the Gaussian part of the multiple-scattering angular distribution increases linearly with depth of penetration, and Lindhard defined a characteristic depth, z_{n,ψ_1}, as the thickness giving a root-mean-square multiple scattering angle equal to ψ_1,

$$Z_{n,\psi_1} = \frac{2}{\pi \, N d^2 L_n \psi_1^2}, \qquad (4.3)$$
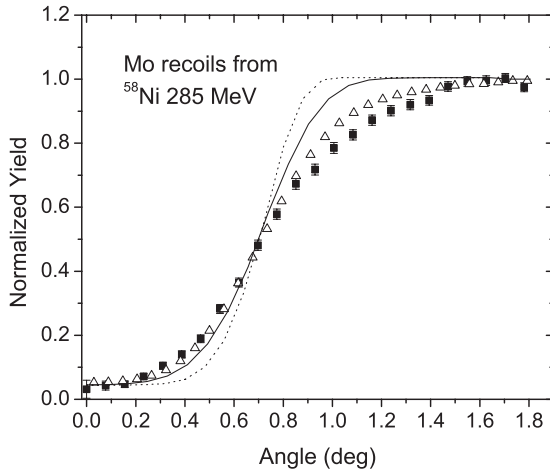
FIG. 6. Blocking dip for 91-MeV Mo recoils from 285-MeV ^{58}Ni. The square black points are from the measurement and the triangles from a binary-collision simulation. The full and dotted curves are from continuum-model calculations with and without the correction for mosaic structure, respectively.
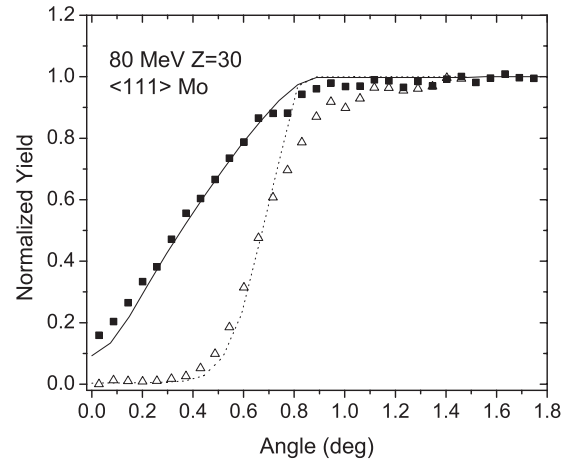

FIG. 7. Comparison of continuum-model calculations with binary-collision simulations for a perfect Mo crystal, without a recoil displacement (dotted) and with an exponential distribution of displacements with average 30 pm (full).

where N is the atomic density of the crystal and L_n the logarithmic factor for nuclear stopping which for the present cases is $L_n \sim 6$ [25]. The magnitude of this length for $\psi_1 = 0.5°$ is about 10 times the thickness of the 200-nm Mo crystal along the direction toward the detector. The scaling with the inverse square of the critical angle implies that multiple scattering is a more important correction for the wider blocking dips for fission fragments than for elastically scattered ions.

To estimate this effect we have measured a blocking dip for Mo recoils from 285-MeV Ni with average energy 90.5-MeV after the elastic scattering. The width of this dip is similar to that of the fission dips. In Fig. 6 the dip is compared with the continuum-model calculation and a calculation without the correction for mosaic spread. The latter correction is smaller than for the narrower elastics dips. The measurements are reasonably well reproduced by a Monte Carlo simulation of binary ion-atom scattering [28] and they deviate from the continuum model calculation mainly in the shoulder region. As expected, this deviation is larger than for the elastic dips in Figs. 5(a)–5(c). There is also a small increase in the yield just inside the dip but, as we shall see, this fill-in is small compared to the effects due to a long-lifetime component for fission fragments.

Figure 6 demonstrates that the binary-collision simulations are a reasonable proxy for the measurement. The accuracy of the simpler (and much faster) analytical calculations, therefore, can be assessed by a comparison with such simulations for parameters similar to those for fission fragments. Such a comparison without the empirical corrections for mosaic structure and interface damage/strain is shown in Fig. 7 for blocking dips without recoil displacement and with an exponential distribution of displacements with average 30 pm perpendicular to the axis, respectively. For zero displacement the agreement is very good except for the shoulder depression discussed above. This difference is smaller for 30 pm average displacement but there is a discrepancy at very small angles. The origin of this discrepancy is blocking of axial-channeling

trajectories by crystal planes containing the axis [26]. As seen in the figure, this effect gives only a very small perturbation of the reduction of the dip volume due to the displacement.

As discussed below, the tail toward long fission times, and, hence, the distribution of recoil distances before fission, can be represented by a sum of exponentials, and, therefore, we may conclude that comparison with analytical calculations, with corrections for mosaic spread, angular resolution, and interface strain, can be used as an accurate method for interpretation of the fission blocking dips.

V. STATISTICAL SIMULATIONS OF FISSION

There are important differences between the fission process for the nuclei created by bombardment of Mo and fission of the heavier nuclei created in our previous experiments with the same ions bombarding a W target. First, the fission barriers are very large at zero angular momentum and the measured yields of evaporation residues are similar to or larger than the fission yields. This is strong evidence for the dominant role of angular momentum. Qualitatively, there is no fission for low angular momentum but beyond a limiting angular momentum the nucleus fissions eventually, maybe after evaporation of a few neutrons.

Second, the RLDM predicts highly deformed barrier configurations. Hence, the fusion of the two nuclei creates a united nucleus with less deformation than at the barrier. This favors formation of a compound nucleus protected by a barrier and in statistical equilibrium before fission. Shape diffusion over a barrier is not required to get complete fusion as for the very heavy systems we studied previously [14].

We use a standard statistical model similar to that described in Ref. [1]. Fission is in competition with neutron emission and this leads to multichance fission with a large spread in lifetimes. The fill-in of the blocking-dip minimum is due to fission after emission of several neutrons (here two to four). For simplicity, we ignore emission of light, charged particles

(protons and α particles), although it is known that this can be a significant channel for the fused nuclei [29–31]. Our aim is mainly to investigate whether the blocking results are consistent with the standard picture of multichance fission and a very broad lifetime distribution.

Fission of nuclei with intermediate fissility was studied experimentally and theoretically in the 1970s and 1980s and a reasonable understanding was achieved. It was based on the predictions of nuclear shapes and energies from the RLDM [15]. Simple approximate formulas are given in Ref. [15] for the surface energy (MeV) of a nucleus with atomic number Z and mass number A,

$$E_S = 17.9439\{1 - 1.7826[(A - 2Z)/A]^2\}A^{2/3}, \quad (5.1)$$

and for the Coulomb energy,

$$E_C = 0.7053(Z^2/A^{1/3}). \quad (5.2)$$

The ratio $x = E_C/2E_S$ is the main dimensionless parameter in the LDM. A second parameter in the RLDM is the ratio of the rotation energy—with the spherical rigid-body moment of inertia—to the surface energy, $y = E_R/E_S$, where E_R is given as

$$E_R = 34.54\frac{I^2}{A^{5/3}}. \quad (5.3)$$

Here I is the angular momentum in units of $\hbar$. Figure 13 of Ref. [15] contains a series of curves specifying the magnitude of the fission barrier as a function of the parameters x and y. For fixed x, the barrier decreases nearly linearly with y, i.e., it decreases linearly with the square of the angular momentum except for a slower decrease close to the critical angular momentum, I_c, where the fission barrier vanishes.

The RLDM barrier has been used in a number of papers analyzing fission cross sections in heavy-ion reactions with medium-Z nuclei [16–19]. All papers refer to the basic work by Cohen *et al*. but there are refined variations of the model and slightly different formulas are given for the basic parameters. It was found that the barriers must be reduced by a factor 0.5–0.7 to get agreement between measurements and statistical-model calculations. An explanation was found in a finite-range correction for the surface energy [20], and there seemed to be reasonable consistency with measurements [21].

We have taken the fusion barrier, B, from the Bass model [32] with $r_0 = 1.2$ fm. The fusion cross section, σ_{CF}, is calculated as [1,2]

$$\sigma_{CF} = (1 - k)\pi r_0^2 \left(A_1^{1/3} + A_2^{1/3}\right)^2 (1 - B/E), \quad (5.4)$$

in most cases with $k = 0$. Figure 8 shows the spin distribution for 240-MeV ^{48}Ti on ^{96}Mo. A slightly smeared spin cutoff has been used but this is not very important. Also the spin dependence of the fission barrier is shown.

To be consistent with the calculations in Refs. [16–19] we have used the level density parameter $a_c = A/8$. At the barrier, the value of a_f is assumed to be higher by a factor 1.03, which decreases to unity at the critical angular momentum, I_c. The precise choice of level density parameters is not of much significance for the magnitude of the long-lifetime component. In contrast, the friction parameter, η, is very important. We have used a constant value of η since we do
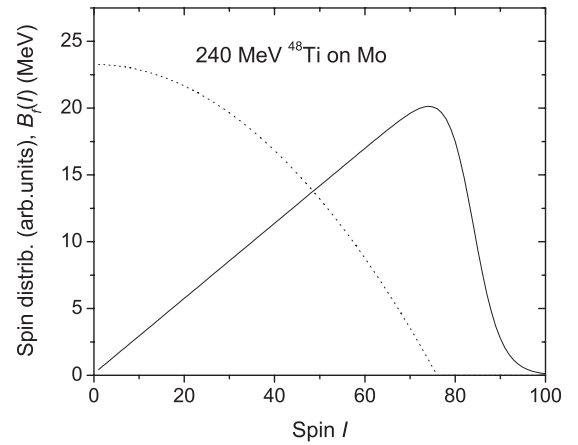

FIG. 8. Spin distribution (full curve) and fission barrier (dotted) for 240-MeV ^{48}Ti on ^{96}Mo.

not have information on the energy dependence from our experiment.

Figure 9 illustrates the influence of η on the distribution of fission over stages in the neutron cascade. It is taken from the calculation for 240-MeV ^{48}Ti on ^{96}Mo and shows the dependence of the fission probability P_f on the thermal excitation energy, $U = E_{\text{exc}} - E_{\text{rot}}$, for the spin values given in the figure. The full curves are for $\eta = 3$ and the dotted ones for $\eta = 0$. In the latter case the fission barrier has been increased by 25% to keep the fission cross section fixed. We see that for $\eta = 3$ P_f is not very large around $I = 60$ and increases strongly with decreasing excitation energy. This favors late-chance fission. For $\eta = 0$ the curves only increase toward lower excitation energy when P_f is already so large that early-chance fission dominates.

The decay is assumed to be a competition between fission and neutron emission and, therefore, the neutron binding energies are important. They are of order 10 MeV but with a significant dependence on mass number. The mass distribution
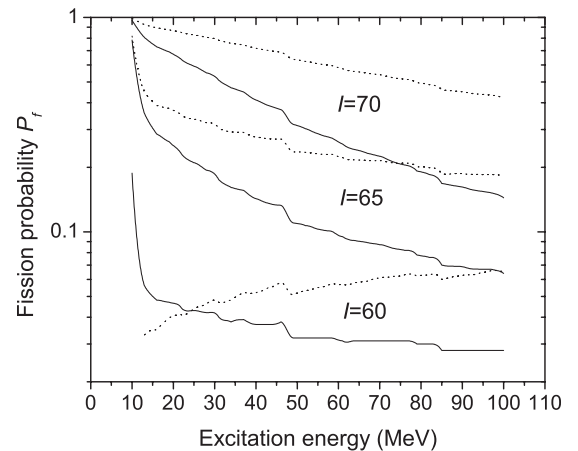

FIG. 9. Fission probability for three spins as a function of excitation energy minus rotation energy, calculated for 240-MeV ^{48}Ti on ^{96}Mo. The dotted curves are for $\eta = 0$ and the full curves for $\eta = 3$. The fission barrier has been multiplied by a factor of 1.24 for $\eta = 0$ to keep the fission cross section the same.
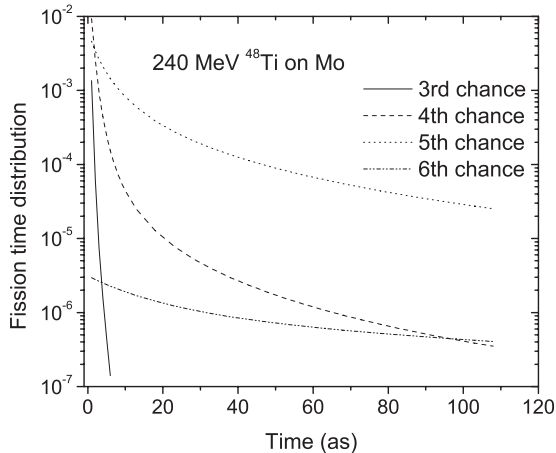
FIG. 10. Fission time distributions at various stages of the neutron cascade, calculated for 240-MeV ^{48}Ti on ^{96}Mo with $\eta = 3$.

for Mo is broad, ranging from 92 to 100 with 74% even-N isotopes and average mass 96. All calculations have been made for mass 96.

There are large odd-even differences in the neutron binding energies given in the NIST tables [33], corresponding to a neutron pairing energy of order 2 MeV. The pairing is believed to disappear for nuclear temperatures above about 1 MeV [34], and the most consistent way to chose neutron binding energies is to eliminate completely the pairing energy. For even-N nuclei the binding is then assumed to be the same as for the nuclei with one neutron less since the number of neutron states at each energy level must be even. For the Ce isotopes (S + Mo), the slope of B_n with decreasing number of neutrons is 0.5 MeV for a pair of neutrons. This slope is only half as large for the Gd isotopes (Ti + Mo) but more than twice as large, 1.2-MeV per neutron pair, for the Yb isotopes (Ni + Mo).

Parameters and results from simulations of the measurements are given in Table I. Except for ^{32}S bombardment, the fission cross sections are reasonably well reproduced. The parameter k in Eq. (5.4) was set equal to zero for the lighter ions but for ^{58}Ni a value $k = 0.15$ was needed to reduce the calculated cross section to the measured value. This may be justified by the fact that the maximum value of the spin is

otherwise much larger than the critical value, I_c, corresponding to $B_f = 0$. This is not the case for ^{32}S bombardment and the discrepancy between measured and calculated cross sections must for this case be found elsewhere, perhaps in the competition from emission of light, charged particles [29–31]. The omission of these channels in the simulations is a deficiency but it appears difficult to include them in a consistent manner [30,31]. Furthermore, the measured α and proton multiplicities are small (a few percent) in coincidence with fission and larger by an order of magnitude for evaporation residues, so inclusion of these channels appears mainly to reduce the fission cross section without much change of the distribution of fission over the evaporation cascade.

The fractions of fission after 1 and 10 as are derived from comparison with the blocking data as discussed in the following section. These numbers characterize the long tail of the time distribution better than a mean lifetime. The long lifetimes stem mainly from fission after evaporation of three and four neutrons, as seen in Fig. 10. A strong influence of viscosity, represented by the parameter η in the table, is needed to bring the simulations in agreement with the blocking data, as discussed in the following section.

For ^{32}S-induced fission, both the finding of a tail of the fission time distribution with lifetimes longer than one attosecond and our conclusion about the importance of viscosity are consistent with the recent, more complete, analysis of similar reactions in Refs. [29–31]. The sensitivity of the long-lifetime component to η is smaller for ^{48}Ti and ^{58}Ni bombardment because there is a high-spin region with very low fission barrier and predominantly first-chance fission. As seen in Table I, this is reflected in higher fission cross sections for these ions.

VI. DATA PRESENTATION

A. Energy spectra

For the identification of fission fragments in the $(\Delta E, E_{rest})$ plots it is important that the energy spectra are consistent with the expectations for fission. The best test is for ^{32}S since there is no interference from Mo recoils so the whole energy spectrum of fission fragments is obtained. The spectrum shown in Fig. 11 for 170 MeV is in good agreement with the mass

TABLE I. Parameters and results of experiments and calculations. The bombarding energy, E, the excitation energy, E^*, and the fission barrier, B_{f0}, at zero angular momentum are given in MeV, and the maximum angular momentum for fusion, I_m, and the critical angular momentum, I_c, with $B_f(I_c) = 0$, are in units of $\hbar$. The calculated cross sections for fusion, σ_{cf}, and for fission, σ_f, as well as the measured fission cross section, σ_{exp}, are given in mb, and the times, τ, in as. The two dimensionless numbers are the viscosity parameter, η, and the calculated number of pre-scission neutrons, ν_{pre}.

Ion	E	E^*	I_m	I_c	B_{f0}	η	σ_{cf}	σ_f	σ_{exp}	$\tau > 1$	$\tau > 10$	ν_{pre}	$\tau > 1$[a]	$\tau > 10$[a]
^{32}S	170	88	65	86	28	1	963	55	32 ± 8	0.21	0.050	1.41	0.10	0.005
^{32}S	180	95	70	86	28	1	1063	175	80 ± 20	0.16	0.032	1.52	0.10	0.017
^{48}Ti	225	84	74	76	30	3	788	189	250 ± 25	0.18	0.061	1.08	0.07	0.016
^{48}Ti	240	94	84	76	30	3	931	367		0.12	0.048	0.80	0.03	0.008
^{58}Ni	285	77	74	68	23	3	583	281	250 ± 25	0.15	0.039	0.85	0.09	0.021
^{58}Ni	300	87	83	68	23	3	693	415	420 ± 40	0.09	0.030	0.74	0.05	0.016

[a]These values obtained for $\eta = 0$, with B_{f0} multiplied by 1.24 to keep the fission cross section roughly constant.
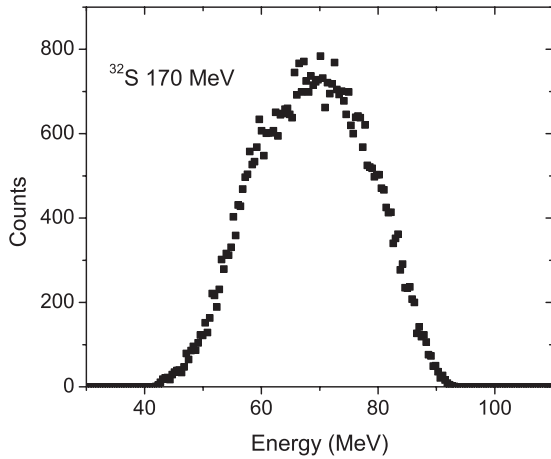
FIG. 11. Fission energy distribution recorded by the gas counter for 170-MeV ^{32}S.

FIG. 12. Energy distributions recorded by the gas counter for 180-MeV ^{32}S for events within the two polygons shown in Fig. 2(a).

and energy spectra obtained in Ref. [29] for fission fragments from 200-MeV ^{32}S on ^{100}Mo. The measured average energy is 68.7 MeV, to which should be added about 3 MeV from stopping in the target, and the result is 2 MeV above the value calculated from a total fission energy release of 46 MeV per fragment [29]. Half of this difference is accounted for by a correction for the dependence on observed fragment energy of the detector solid angle in the frame of the fissioning nucleus so the agreement is quite good. The energy release from Viola systematic [35] is slightly smaller (43.3 MeV), and we have used the correction from Ref. [29] to this value. Similar small corrections have been applied to the Viola values for the heavier bombarding ions. The energy release is used in the analysis of blocking to derive the mass (and charge) of the fragments from their energy via the collision kinematics, as discussed in Sec. III.

As seen in Figs. 2(b) and 2(c), the elastic Mo recoils overlap with the low-energy fission fragments for the heavier projectiles, and, therefore, only the high-energy fragments can be used in the blocking analysis of fission lifetimes. To check that this limitation does not affect the blocking analysis we have for 180-MeV ^{32}S defined two regions with the polygons shown in Fig. 2(a). The corresponding energy spectra are shown in Fig. 12. The blocking analyses for the two regions are discussed below.

The energy spectra defined by the polygons in Figs. 2(b) and 2(c) for ^{48}Ti and ^{58}Ni bombardment are shown in Fig. 13. In both cases the lower cutoff is close to the predicted average fragment energy. The number of fragments detected is much lower for 300-MeV ^{58}Ni and to get sufficient statistics, we have used half the angular resolution in the blocking analysis. For 285 MeV the fission yield was too low for a blocking analysis but the elastic-scattering yield was sufficient [Fig. 5(c)].

B. Fission cross sections

The fission cross sections were not determined very accurately in the experiment but estimates are given in Table I. In all cases the scattering angle of 54° is larger than or close to the cut-off angle for Rutherford scattering, so the elastics
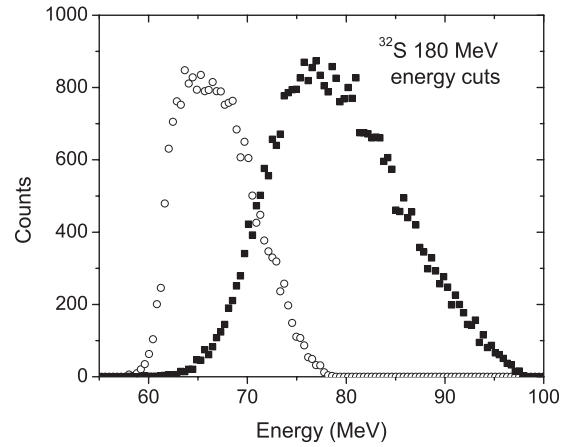
cannot be used for normalization. For ^{32}S bombardment we have used data from a previous experiment [3] with a thin epitaxial layer of W on top of the Mo crystal to estimate the Mo-fission cross sections from comparison with elastic scattering from W. We have assumed a $1/\sin\theta$ distribution of fragments in the center-of-mass system, where θ is the angle of emission relative to the beam direction. The large uncertainties stem mainly from energy-loss corrections. In addition, the yield of elastic Mo recoils can be used as a reference in some cases. For ^{48}Ti at 225 MeV the scattering angle associated with the Mo recoils is smaller by a few degrees than the grazing angle corresponding to a decrease of the scattering cross section by a factor of 4 relative to the Rutherford cross section. The value of the measured fission cross section given in Table I is calculated using the Rutherford scattering cross section and we have assumed the real fission cross section to be somewhat smaller. As it turns out, the value of the viscosity parameter η obtained from a fit to the fission blocking dip depends only weakly on the magnitude of the fission barrier, and, hence, the uncertainty of the fission cross section is not so important. The comparison with Mo recoils has also been used to estimate the fission cross section for ^{58}Ni bombardment
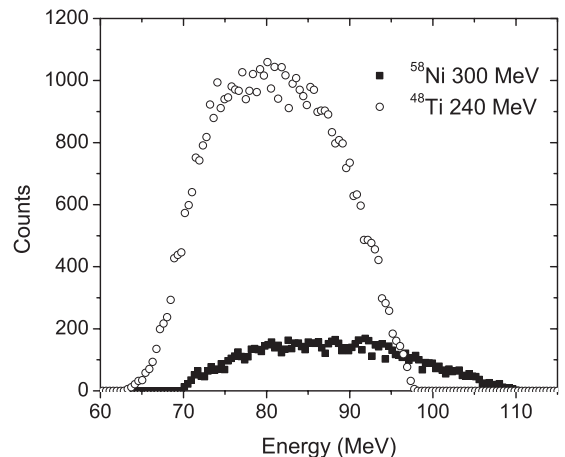

FIG. 13. Energy distributions for 240-MeV ^{48}Ti and 300-MeV ^{58}Ni for events within the polygons shown in Figs. 2(b) and 2(c).
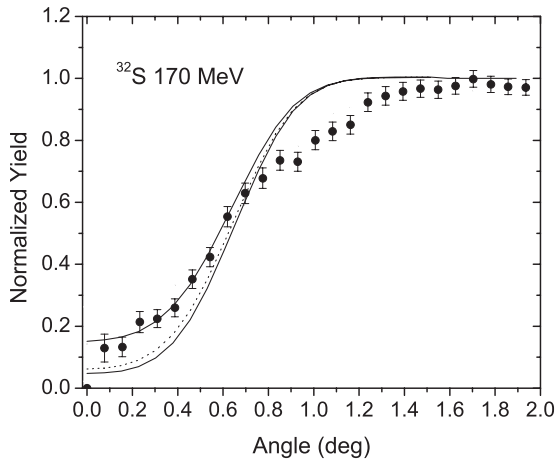
FIG. 14. Fission blocking dip for 170-MeV ^{32}S. The lower curve is from a continuum-model calculation without recoil displacement and the two other curves with recoil displacements corresponding to the calculated time distribution for $\eta = 1$ (full) and $\eta = 0$ (dotted).

where the separation of the scattering angle from the grazing angle is larger.

For the Ti and Ni bombarding ions the calculations reproduce the measured cross sections with reasonable parameters. However, there is a large discrepancy for the two measurements with ^{32}S. We note that our estimated experimental values in Table I are in reasonable accord with the 130 mb measured for 200 MeV ^{32}S on ^{100}Mo [31]. The discrepancy of the calculated cross sections from the measured ones is difficult to remove by adjustment of parameters in the statistical model. If the fission barrier is increased the cross sections are reduced but their energy dependence becomes even steeper. As mentioned above, an explanation may perhaps be found in the competition with emission of protons and α particles, which has not been included in the calculations.

C. Blocking dips for fission fragments

The blocking dips for ^{32}S bombardment at 170 and 180 MeV are shown in Figs. 14, 15(a), and 15(b). The minimum yield is clearly higher than for the calculation without recoil displacement while the width is not much narrower, signaling the presence of a long-lifetime component in the fission decay. Good agreement is obtained in all cases with a time distribution calculated with the parameters given in Table I for $\eta = 1$ but not without the correction for viscosity ($\eta = 0$). The widths of the two dips for 180 MeV, corresponding to the energy distributions in Fig. 11(b), scale with energy as calculated from Eq. (4.2) with average-E values from the spectra in Fig. 9 and Z_1 values from the kinematics. The consistent fits to the two dips confirm that the energy cuts required for the heavier bombarding ions are not a problem for the lifetime determination. There is for all dips a discrepancy from the calculations just outside the dip that, as discussed in Sec. IV, is caused by multiple scattering in the Mo crystal.

The blocking dips for ^{48}Ti bombardment shown in Figs. 16(a) and 16(b) also demonstrate the presence of a long-lifetime component, and a larger value of the viscosity
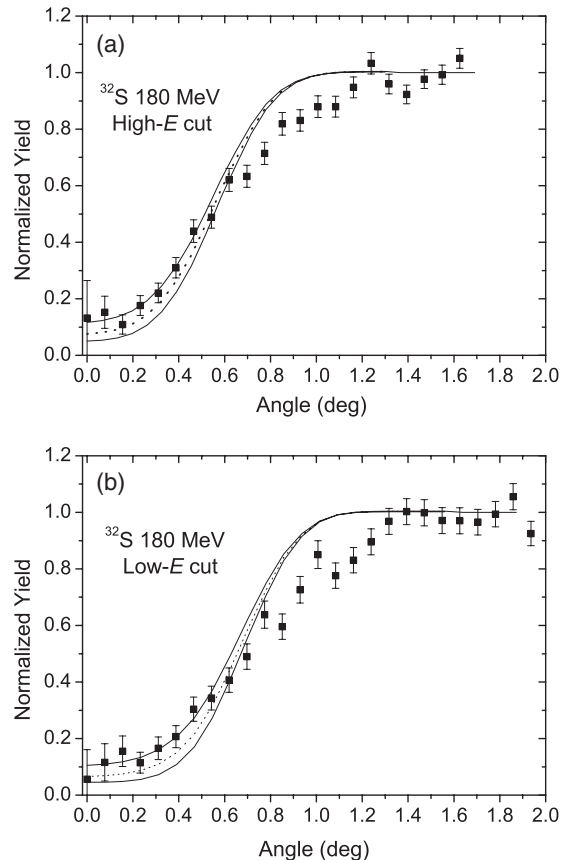

FIG. 15. As Fig. 14 but for fission events defined by the two polygons in Fig. 2(a) for 180-MeV ^{32}S.

parameter is needed to reproduce the dips (Table I). The large increase in minimum yield without a corresponding narrowing of the dips provides clear evidence of non-exponential decay, with most fissions happening at times much shorter than 1 as and a tail of the time distribution toward much longer times. The time distribution obtained from the calculation for 240 MeV with $\eta = 3$ was fitted very well with a sum of five exponential components (79.5% $\tau = 0$ as, 10% $\tau = 1$ as, 3.9% $\tau = 7$ as, 3.8% $\tau = 24$ as, and 2.8% $\tau = 100$ as), and similar representations were used for all the blocking calculations. The four lifetimes were chosen to give a good representation of the calculated distribution and have no special physical significance.

The measurements with a ^{58}Ni beam have rather poor statistics, and only for 300 MeV were the statistics sufficient for blocking analysis with the size of the angular bins increased by a factor of 2. The resulting dip is shown in Fig. 17. There is less fill-in of the dip minimum and the statistics of the data do not allow a distinction between the calculations for $\eta = 0$ and $\eta = 3$. There is also very little narrowing of the dip from lifetime effects. The stronger dominance of very short lifetimes for this case may be explained qualitatively by the larger contribution to the fission cross section from nuclei with angular momentum larger or of order of the critical spin I_c where the fission barrier vanishes (see Table I).

FIG. 17. Fission blocking dip for 300-MeV ^{58}Ni, for events within the polygon shown in Fig. 2(c). Calculated curves without recoil and with displacement distributions calculated for $\eta = 3$ (full) and $\eta = 0$ (dotted).
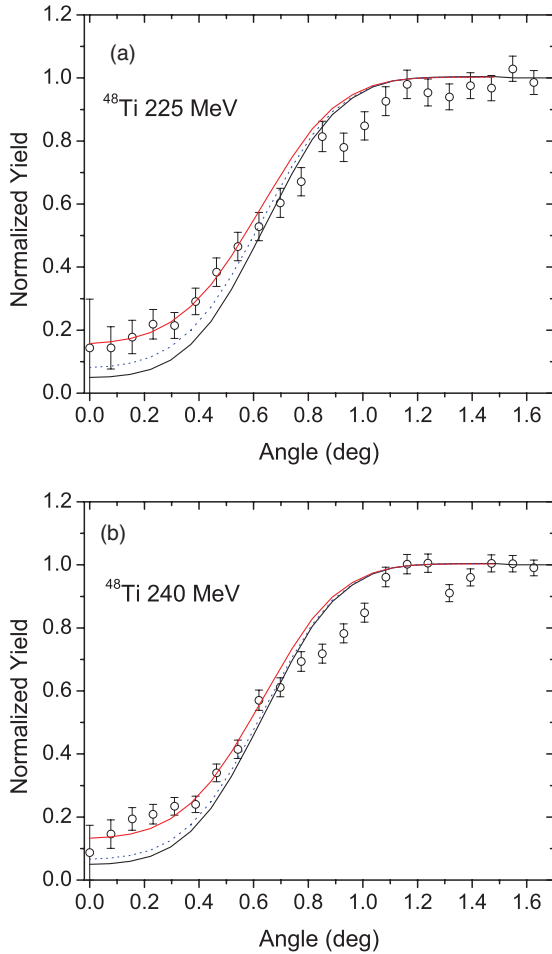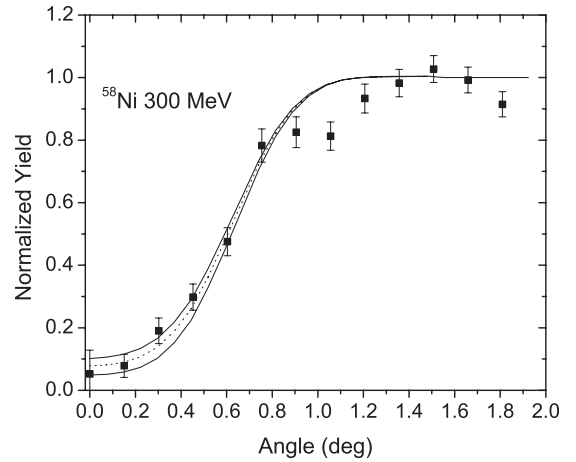
FIG. 16. (Color online) Fission blocking dips for ^{48}Ti at 225 MeV (a) and 240 MeV (b). The curves are calculated without recoil displacement (lower full) and with the displacement distributions from a statistical model with $\eta = 3$ (full) and $\eta = 0$ (dotted).

VII. DISCUSSION AND CONCLUSIONS

The measurements presented here have demonstrated that the time scale of heavy-ion-induced fission of fused nuclei in the intermediate-Z region, $Z \sim 60$–70, is consistent with the standard Bohr-Wheeler picture of compound nucleus formation followed by a cascade of neutron emission in competition with fission. This description has also been used successfully to interpret earlier crystal-blocking measurements for fission induced by bombardment with light ions (^{12}C, ^{16}O, ^{19}F). From the observed angular widths of the fragment blocking dips it is concluded that most of the fissions happen on a time scale that is too short to give a nuclear recoil influencing the crystal blocking of fragments, but there is, in most cases, a significant fill-in of the minimum of the blocking dips, revealing a long-lifetime component from late-stage fission (attoseconds or more).

Such results are not dependent on statistical modeling but can be interpreted by comparison with the outcome of modeling. We find that our data can be reproduced within the Bohr-Wheeler picture by inclusion of a Kramers correction for nuclear viscosity ($\eta \sim 1$–3) in a standard statistical model. It

should be noted that the magnitude of the viscosity parameter derived from blocking experiments or from measurements of pre-scission neutrons is model dependent. A recent, more advanced theoretical description of fission induced by light-ion bombardment indicates that the viscosity parameter may often be overestimated [36]. Also, our statistical model is rather simple and does not include emission of light, charged particles which has been shown to be an important channel [29–31]. However, in these more complete studies of reactions similar to ours a very similar contribution from late-chance fission with long lifetimes was found [29].

The main purpose of the present study was to investigate more general, basic features of fission dynamics. In our recent measurements with the same setup of heavy-ion-induced fission of much heavier and more fissile nuclei ($Z = 96$ and 102), the decay was found to be exponential with a single lifetime of order 1 as, and this is not consistent with the standard Bohr-Wheeler picture of multichance fission. We interpreted the results as fission without formation of a compound nucleus, delayed by nuclear viscosity, "fission by diffusion" [3,13] analogous to the "fusion by diffusion" in Ref. [14]. One example of these measurements is shown in Fig. 18. In contrast to the present measurement for 300 MeV ^{58}Ni on Mo (Fig. 17)—and also to the measurements with other ions bombarding a Mo target—there is a strong narrowing of the fission blocking dip compared with the calculation for zero lifetime. The measured dip is fitted perfectly by a calculation for exponential decay with lifetime 1.4 as (the small excess yield at the dip center is expected, cf. the discussion of Fig. 7).

This result was challenged in a recent letter on the basis of measurements of correlated mass and angular distributions of fragments in nearly the same heavy-ion reactions, ^{48}Ti and ^{64}Ni bombarding W targets [37]. It was claimed that the results reported there show the dominant reaction to be quasifission happening typically before the system formed has made half a rotation. The argument was based on a figure showing the correlation between fragment mass and emission angle. The strong deep inelastic scattering at forward and
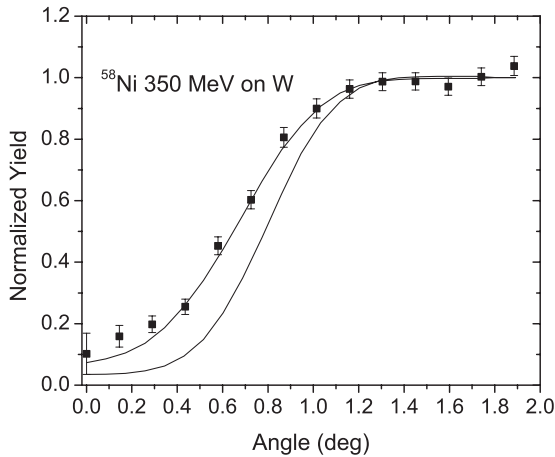
FIG. 18. Fission blocking dip for 350-MeV ^{58}Ni on W (from Ref. [3]). The curves are calculated without recoil displacement and with an exponential distribution of displacements corresponding to a lifetime of 1.4 as, respectively.

backward angles, with a very asymmetric mass distribution, gives the impression of a strong correlation between mass and angle for all fragments. However, it was not established in the letter that this correlation holds for all fragments. In our experiment the detector collected fragments at close to 90° in the center-of-mass system, where the intensity of inelastic scattering is lowest, and we discriminated against inelastic scattering by a cut in the energy spectrum, as shown in Fig. 2.

It is well established that, except for very heavy collision partners, deep inelastic scattering is confined to the largest impact parameters and angular moments [38]. The projectile nucleus is captured by the attractive nuclear forces and slides at the surface of the target nucleus with rapid dissipation of kinetic energy but limited mass exchange, and the collision partners separate within the first half-revolution. For smaller impact parameters, the relative motion is stopped and the sliding is replaced by sticking. The centrifugal repulsion is reduced and the fused nucleus is stable over many revolutions until it fissions with a nearly symmetric mass split. Figure 2 of Ref. [3] shows, for both ^{48}Ti and ^{58}Ni on W, an intensity minimum between fragments from nearly symmetric fission and projectile-like fragments from deep inelastic scattering, and this allowed us to discriminate against the latter. Furthermore, the long time scale of the fission process is reflected not

only in narrower fragment blocking dips but also in emission of a number of pre-scission neutrons, as discussed for similar reactions in Ref. [13].

The present experiment helps eliminate speculation that our earlier observation of attosecond lifetimes for heavy-ion-induced fission in a W target is an artifact of the blocking technique [37]. With the same setup and analysis we have observed blocking dips for fragments from heavy-ion-induced fission in a Mo target without the strong narrowing of the dips observed earlier for fission fragments from bombardment of W. Also, the suggestion in Ref. [37] that recoil from neutron emission from fragments could be responsible for the narrowing can be dismissed. As argued in detail in Ref. [3], such recoils cannot cause the dip narrowing seen in Fig. 18.

Thus, our experiment on heavy-ion-induced fission of Mo has confirmed and strengthened the conclusion that the heavy-ion-induced fusion-fission process undergoes a fundamental change for very large charge and mass of the fissioning nucleus. The standard Bohr-Wheeler picture of competing quantum transitions in a compound nucleus is replaced by a more classical picture with fission dynamics decoupled from neutron emission [13]. The fusion-fission proceeds without formation of a compound nucleus, and the delay is caused by strong damping of the deformation toward scission.

Crystal blocking of fission fragments has also been measured for heavy-ion reactions producing superheavy elements, and the results indicate attosecond lifetimes also in these reactions [39]. The data have been interpreted in the standard Bohr-Wheeler picture and claimed to indicate stability of superheavy compound nuclei protected by a fission barrier. In view of our results for heavy-ion-induced fission in a W target, this interpretation may have to be revised. The theoretical study in Ref. [14] indicates that the picture of fusion by diffusion can be extended to such reactions and this may also hold for our picture of fission without formation of a compound nucleus, delayed by the high viscosity of nuclear matter and not by a high fission barrier.

ACKNOWLEDGMENTS

[1] S. A. Karamian, J. S. Forster, J. U. Andersen, W. Assmann, C. Broude, J. Chevallier, J. S. Geiger, F. Grüner, V. A. Khodyrev, F. Malaguti, and A. Uguzzoni, Eur. Phys. J. A **17**, 49 (2003).

[2] J. U. Andersen, J. Chevallier, J. S. Forster, S. A. Karamian, C. R. Vane, J. R. Beene, A. Galindo-Uribarri, J. Gomez del Campo, H. F. Krause, E. Padilla-Rodal, D. Radford, C. Broude, F. Malaguti, and A. Uguzzoni, Phys. Rev. Lett. **99**, 162502 (2007).

[3] J. U. Andersen, J. Chevallier, J. S. Forster, S. A. Karamian, C. R. Vane, J. R. Beene, A. Galindo-Uribarri, J. G. del Campo, C. J. Gross, H. F. Krause, E. Padilla-Rodal, D. Radford,

D. Shapira, C. Broude, F. Malaguti, and A. Uguzzoni, Phys. Rev. C **78**, 064609 (2008).

[4] W. M. Gibson, Annu. Rev. Nucl. Sci. **25**, 465 (1975).

[5] S. A. Karamian, Yu. Ts. Oganessian, and F. Normuratov, Yad. Fiz. **14**, 499 (1971).

[6] V. V. Kamanin, S. A. Karamian, F. Normuratov, and S. P. Tretyakova, Yad. Fiz. **16**, 447 (1972).

[7] V. N. Bugrov and S. A. Karamian, Yad. Fiz. **40**, 857 (1984).

[8] J. U. Andersen, E. Lægsgaard, K. O. Nielsen, W. M. Gibson, J. S. Forster, I. V. Mitchell, and D. Ward, Phys. Rev. Lett. **36**, 1539 (1976).

[9] J. U. Andersen, A. S. Jensen, K. Jørgensen, E. Laegsgaard, K. O. Nielsen, J. S. Forster, I. V. Mitchell, D. Ward, W. M. Gibson, and J. J. Cuomo, Mat. Fys. Medd. Dan. Vid. Selsk. **40**, No. 7 (1980).

[10] J. S. Forster, I. V. Mitchell, J. U. Andersen, A. S. Jensen, E. Laegsgaard, W. M. Gibson, and K. Reichelt, Nucl. Phys. A **464**, 497 (1987).

[11] J. U. Andersen, N. G. Chechenin, A. S. Jensen, K. Jørgensen, and E. Lægsgaard, Nucl. Phys. A **324**, 39 (1979).

[12] N. Bohr and J. A. Wheeler, Phys. Rev. **56**, 426 (1939).

[13] K. Siwek-Wilczynska, J. Wilczynski, R. H. Siemssen, and H. W. Wilschut, Phys. Rev. C **51**, 2054 (1995).

[14] W. J. Swiatecki, K. Siwek-Wilczynska, and J. Wilczynski, Phys. Rev. C **71**, 014602 (2005).

[15] S. Cohen, F. Plasil, and W. J. Swiatecki, Ann. Phys. **82**, 557 (1974).

[16] F. Plasil and M. Blann, Phys. Rev. C **11**, 508 (1975).

[17] M. Beckerman and M. Blann, Phys. Rev. Lett. **38**, 272 (1977).

[18] B. Sikora, W. Scobel, M. Beckerman, J. Bisplinghoff, and M. Blann, Phys. Rev. C **25**, 1446 (1982).

[19] M. Blann and T. T. Komoto, Phys. Rev. C **26**, 472 (1982).

[20] H. J. Krappe, J. R. Nix, and A. J. Sierk, Phys. Rev. **20**, 113 (1979).

[21] M. Blann, Phys. Rev. C **34**, 2215 (1986).

[22] H. Hofmann and D. Kiderlen, Phys. Rev. C **56**, 1025 (1997).

[23] H. Kramers, Physica (Amsterdam) **7**, 284 (1940).

[24] W. Assmann, H. Huber, C. Steinhausen, M. Dobler, H. Gluckler, and A. Weidinger, Nucl. Instrum. Methods B **89**, 131 (1994).

[25] J. Lindhard, K. Dan. Vid. Selsk. Mat. Fys. Medd. **34**, No. 14 (1965).

[26] J. U. Andersen and A. Uguzzoni, Nucl. Instrum. Methods B **48**, 181 (1990).

[27] J. U. Andersen, B. Bech Nielsen, A. Uguzzoni, E. Fuschini, E. F. Kennedy, and V. A. Ryabov, Nucl. Instrum. Methods B **90**, 166 (1994).

[28] E. Fuschini, F. Malaguti, A. Uguzzoni, and E. Verondini, Rad. Eff. **81**, 37 (1984).

[29] P. N. Nadotchy, A. Brondi, A. Di Nitto, G. La Rana, R. Moro, E. Vardaci, A. Ordine, A. Boiano, M. Cinausero, G. Prete, V. Rizzi, and F. Lucarelli, EPJ Web of Conferences **2**, 08003 (2003).

[30] E. Vardaci, A. Di Nitto, A. Brondi, G. La Rana, R. Moro, P. N. Nadotchy, M. Trotta, A. Ordine, A. Boiano, M. Cinausero, E. Fioretto, G. Prete, V. Rizzi, D. Shetty, M. Barbui, D. Fabris, M. Lunardon, G. Montagnoli, S. Moretto, G. Viesti, N. Gelli, F. Lucarelli, G. N. Knyazheva, and E. M. Kozulin, Eur. Phys. J. A **43**, 127 (2010).

[31] A. Di Nitto, E. Vardaci, A. Brondi, G. La Rana, R. Moro, P. N. Nadotchy, M. Trotta, A. Ordine, A. Boiano, M. Cinancero, E. Fioretto, G. Prete, V. Rizzi, D. V. Shetty, M. Barbui, D. Fabris, M. Lunardon, G. Montagnoli, S. Moretto, G. Viesti, N. Gelli, F. Lucarelli, G. N. Knyazheva, and E. M. Kozhulin, Eur. Phys. J. A **47**, 83 (2011).

[32] R. Bass, Nucl. Phys. A **231**, 45 (1974); J. P. Blocki, H. Feldmaier, and W. J. Swiatecki, *ibid.* **459**, 145 (1986).

[33] G. Audi, A. H. Wapstra, and C. Thibault, Nucl. Phys. A **729**, 337 (2003), available on the internet as NIST Standard Reference Database 144.

[34] D. J. Dean and M. Hjorth-Jensen, Rev. Mod. Phys. **75**, 607 (2003).

[35] V. E. Viola, K. Kwiatkowski, and M. Walker, Phys. Rev. C **31**, 1550 (1985).

[36] S. G. McCalla and J. P. Lestone, Phys. Rev. Lett. **101**, 032702 (2008).

[37] R. du Rietz, D. J. Hinde, M. Dasgupta, R. G. Thomas, L. R. Gasques, M. Evers, N. Lobanov, and A. Wakhle, Phys. Rev. Lett. **106**, 052701 (2011).

[38] K. Siwek-Wilczynska and J. Wilczynski, Nucl. Phys. A **264**, 115 (1976).

[39] M. Morjean, D. Jacquet, J. L. Charvet, A. L'Hoir, M. Laget, M. Parlog, A. Chbihi, M. Chevallier, C. Cohen, D. Dauvergne, R. Dayras, A. Drouart, C. Escano-Rodriguez, J. D. Frankland, R. Kirsch, P. Lautesse, L. Nalpas, C. Ray, C. Schmitt, C. Stodel, L. Tassan-Got, E. Testa, and C. Volant, Phys. Rev. Lett. **101**, 072701 (2008).